Received: August 21, 2022. Revised: September 10, 2022. 392

International Journal of
Intelligent Engineering & Systems

http://www.inass.org/

Liver Multi-class Tumour Segmentation and Detection Based on Hyperion Pre-trained Models

Mina Ibrahim[1]* Muhammad Mahmoud[2] Reda M. Albadawy[3] Hatem Abdulkader[4]

[1]*Department of Information Technology, Faculty of Computers and Information, Menoufia University, Shebin El-kom 32511, Menoufia, Egypt*
[2]*Department of Information Systems, Higher Institute of Management and Technology, Shabramant 12947, Egypt*
[3]*Hepatology, Gastroenterology, Banha University*
[4]*Department of Information Systems, Faculty of Computers and Information, Menoufia University, Shebin El-kom 32511, Menoufia, Egypt*
* Corresponding author's Email: mina.ibrahim@ci.menofia.edu.eg

Abstract: Liver cancer is a common type of cancer that causes death, because there are no noticeable symptoms at an early stage, as this disease is not detected in most patients until cancer has reached the advanced stage only. Researchers are developing algorithms that doctors can use to detect liver tumours early by examining images of tissue from a biopsy or an abdominal medical image. The tissue expert must put in the time and effort required at this stage to determine whether or not this tumour is cancerous and in need of treatment. This model can then be used by a histology expert to make an initial diagnosis. Convolutional neural networks (CNNs) are employed in this paper to propose a novel combination of deep learning models that can transfer information from previously trained global models. After that, this information was decanted into a solo model to improve our model approaches to increase the performance in time and accuracy with tuning to an encoder, decoder, shortcuts, and skip connections to custom convolution layers for three classes such as background, origin, and Tumour shape. Regarding semantic segmentation, our model has proved to be a highly effective way to make results more accurate and valuable to assist in the diagnosis of the liver Tumour using CT scans. As a result, we were able to develop a hybrid model that is capable of recognizing CT images of a liver tumour. Our research yielded the greatest possible results, which we got, reaching 99.50% accuracy, a 86.40% precision and a recall of 97.90%. This accuracy with multi-class is higher than that obtained using other previous models that obtained the best accuracy of 0.991 during the annual periodic examination campaigns for liver cancer detection. Using this model, experts in this field can save time and effort while becoming more informed choices. It also keeps the time and effort that would otherwise be required to administer this treatment, especially during the annual examination campaigns.

Keywords: CT, CNN, Data augmentation, Deep learning, Liver cancer, Multi-class segmentation, Transfer learning, Tumour detection.

1. Introduction

Liver cancer is amid the most prevalent kinds of malignant illnesses, and it was responsible for the deaths of 745,000 people globally in 2012 [1]. Statistics from 2018 indicate that liver cancer is one of the leading causes of mortality. It ranked third in terms of the number of deaths, as it achieved 84,000 deaths despite the high ways of cancer in general and the high cure rates for many diseases and their impact on cancer. However, the rate of cancer has increased. The liver is among the most often affected organs by cancer Tumour metastases, and computed tomography (CT) remains one of the most commonly utilized imaging modalities for the detection, diagnosis, and monitoring of hepatic lesions [2]. A CT scan of the abdomen might be performed useful in the early identification of a variety of different types of liver cancer, including

pancreatic cancer. The procedure may also give exact statistics for the size, shape, and position of any cancerous Tumour s in the liver or elsewhere in the abdomen, as well as details on the blood vessels that surround the tumors. Intravenous injection of a contrast agent before and after, images are captured, with the portal phase images (taken 60–80 seconds after the injection) providing the best identification of lesions. It is necessary to know the precise size, shape, and location of the lesions in order to administer these treatments. The radiologist must spend time reviewing a 3D CT image with numerous lesions in order to manually detect and segment the lesions. Given the complexity of this job, it emphasizes the necessity of computer-aided analysis to help physicians detect and evaluate the size of liver metastases in CT images. Due to the differences in contrast enhancement behaviour between liver lesions, automatic identification and segmentation of liver lesions and parenchyma is a challenging job. Furthermore, due to individual variations in perfusion and scan time, the image contrast between these tissues may be poor.

We present a novel method for creating deep learning methods in the area of liver tumour detection and segmentation using artificial intelligence (AI) to address these issues. The detection centred on the effect of combining a pre-trained VGG16 and ResNet50 architectures in the first portion of our model for feature extraction. After that, we employed transfer learning and fine-tuning techniques using the CNN's architecture via the UNet++ architect and custom layers to get multi-class segmentation accuracy to segment *three* classes: background, origin, and tumor. Consequently, the significance of our research lies in the incorporation of multiple hypered pre-trained models into CNN layers, such as DeeplapV2 and V3, VGG-16, ResNet-50 and UNet++ to detect liver tumours. The principal contributions of this study can be summed up as:

- Propose a novel Hyperion pre-trained models and hypered architect that makes use of CNNs for liver multi-class segmentation and Tumour detection. Our model analyzes whole images rather than patches, which eliminates the need to pick representative patches, avoids unnecessary computations when patches overlap and allows our network to scale up to more effectively as image quality increases.
- As a result of the small size of the used dataset, we have turned to data augmentation by applying scale transformations to the readily available training images. The scale transformations enable the network to learn how to change the texture characteristics of the immediate environment.
- For the purpose of liver segmentation, we employ a fully convolutional architecture and compare it to a patch-based CNN for the detection of liver metastases in CT scans. To our knowledge, this is the first study to segment the liver and identify lesions using a full CNN combination.
- Demonstrate an accurate system that outperforms other previous methods on small datasets and solves the overfitting issue.

The remaining sections are grouped as follows: The recent work is discussed in Section 2. Section 3 illustrates the proposed method adopted in this work. Experimental results and analysis are shown comprehensive discussion in Section 4. The paper is concluded with discussion of future works in Section 5.

2. Related work

In this section, we discuss in detail the approaches currently in use related to liver cancer detection, segmentation, or classification. The previous methods are classified into two categories, such as machine learning [3, 4] and deep learning approaches [5-12]. However, the authors have only included deep learning-related approaches in accordance with the scope of this work. In addition, several recent reviews [13, 14] in this field demonstrate that deep learning has been the focus of nearly all recent liver cancer detection efforts. Havaei *et al*. [5] presented a segmentation network to glioblastomas (brain tumors) by using MRI images. They simultaneously exploited both local and global contextual characteristics. However, they focused on improving the processing time, not on accuracy, using traditional CNN. Dong *et al*. [6], demonstrated the use of hybridized complete CNN for the identification and segmentation of liver cancer utilizing a deep learning algorithm. Numerous layers were employed as feature extractors, and the extracted features were combined with multiple slices. However, they were able to diagnose cancer with a low accuracy of .09722. Sureshkumar *et al*. [7], demonstrated a liver Tumour detection system based on deep learning algorithms. They used a Probabilistic Neural Network (PNN), one of the deep approaches, to recognise and diagnose liver cancers. They discovered that the PNN approach outperformed other machine learning methods in terms of overall accuracy while just

using a few features. However, this method is slower than other neural network models when classifying new cases and require more memory space for the processing. Kaur *et al*. [8], used 3D CT images of liver cancer to demonstrate a multi-organ classification approach based on CNN. To cut down on the computing burden of deep learning, they devised this approach. Data augmentation approaches yielded a good precision of 99.1%. However, this method is Computational complexity and suffer from overfitting problem. Shukla *et al*. [9], presented a cascaded CNN approach for liver cancer detection. First, they partition the liver from end to end in order to limit the likelihood of a mistake occurring during training. After that, they use the liver segmentation images to apply the approach described. The approach they used yielded a low precision of 94.21%. Therefore, this method is not robust and obtain low performance with big and small data. A deep learning-based bio-inspired method for the detection of liver cancer was introduced by Ghoniem [10]. The author used a hybrid segmentation strategy based on multiple models, including optimization using artificial bee colony and UNet Network, for liver lesions extraction from CT images. For extracting the features and classification, the author used a hybrid method that was 98.5% accurate. This method obtained a good result on big data, however, the method obtained very low classification results when working on small data. Zhou and Siddiquee [11] presented UNet as a new network architect called UNet++ for medical image segmentation. centred on a densely supervised encoder-decoder network with nested, dense skip pathways connecting the encoder and decoder sub-networks. In addition, they asserted that the optimizer would handle a learning task when the feature maps of the decoder and encoder networks are roughly equivalent and achieved 92.52% accuracy for cell nuclei, 32.12% accuracy for colon polyps, 82.90% accuracy for liver, and 77.7% accuracy for lung nodules. Ronneberger *et al*. [12] presented a classic UNet network and training based on data augmentation for liver segmentation. An expansive path (right) and a contracting path (left) are both present in the network architecture (right side). The contracting route follows the design of a typical convolutional network. It entails applying two 3×3 convolutions (unpadded convolutions) repeatedly, followed by a rectified linear unit (ReLU) for each one, and down-sampling, up-sampling, and binary class segmentation of a 512×512 image. A segmentation accuracy of 92.03% was attained. This method obtained a very low segmentation accuracy.

A novel and efficient integration technique for the detection of liver tumors is presented in this paper to overcome the issues of the previous works. The proposed method outperforms the majority of existing algorithms on both small and large datasets. Additionally, compared to earlier low-resource deep learning methods for liver detection, our approach is more durable.

3. Methodology

Our new model is explained in this section in details. In addition, all datasets used to evaluate the proposed models are discussed in this section in details. Figure 1 displays the central block diagram of the proposed technique with LiTS NII files CT scans, and 3D-IRCADb-01 dicom CT scans as combined dataset input.

3.1 Liver cancer datasets

3.1.1. First dataset LiTS17

In this study, the liver Tumour segmentation benchmark, LiTS17 [15], is employed. There are 130 CT scans and 70 CT scans for training and testing, respectively in this data set. LiTS dataset NII files containing 3D abdomen image formatted as CT scans images and masks. We prepare dataset CT scans sliced 3d NII volumes CT scan into 2D image slices training set and testing set to JPEG, PNG images to easily train and testing our model.

3.1.2. 3D-IRCADb-01 dataset

Twenty 3D CT scans from twenty liver cancer patients make up this dataset [16]. In each CT image, the liver's average density ranges from 40 to 135, and the resolution is 512x512. Masks images are divided into discrete DICOM segments. A total of 20% of the CT scan images were used in this study as testing and validating sets. That is, using Python libraries, a random sample of 26 CT images was chosen. Ten percent of the dataset's images were disassembled for testing as a final step. After separating the test sample, 80% of the images for the training set were saved, and 10% of the remaining images were saved for validating. Thus, we had 80% training, 10% testing, and 10% validating images.

3.2 Data pre-processing

This stage is divided into two main steps: slicing datasets and data augmentation.

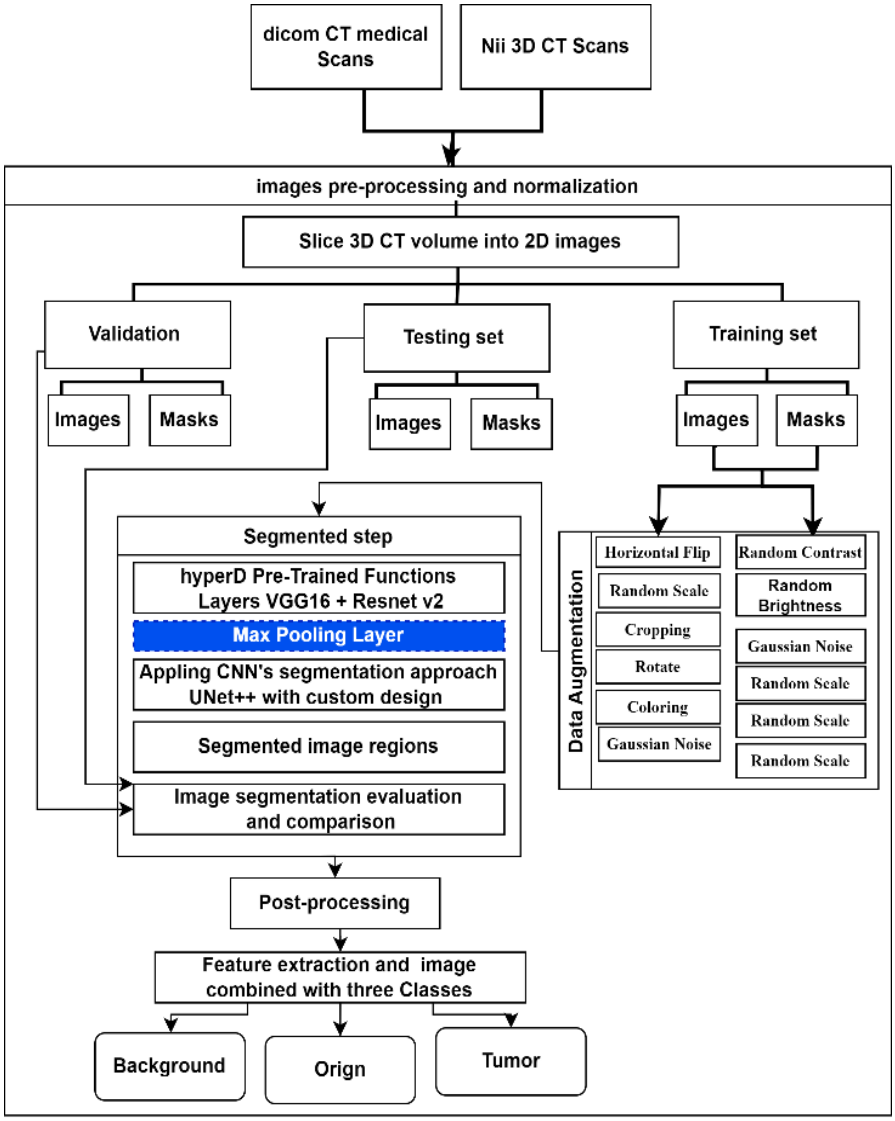

Figure. 1 Central block diagram of the proposed technique

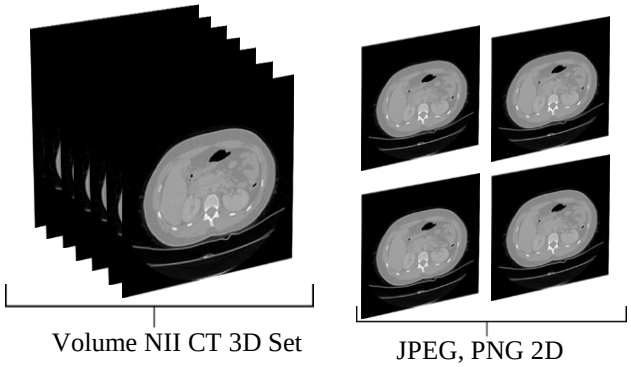

Figure. 2 Slicing 3D volume to 2D JPEG, and PNG images

3.2.1. Slicing datasets

LiTS dataset NII files and 3D-IRCADb-01 dataset Dicom files containing 3D abdomen image formatted as CT scans images trains and masks, we prepare dataset CT scans sliced 3d NII volumes, and Dicom CT scans into 2D image slices training set, validating set, and testing set to JPEG, PNG images to easily train and test our model. Fig. 2 shows slicing 3D volume to 2D JPEG, and PNG images.

3.2.2. Data augmentation

By replacing some of the training images with new ones created using the data augmentation approach, which relies on the following attributes, the training dataset was improved to enable the proposed network to see a wider variety of tumors. We apply the following techniques: Random Contrast, Random Brightness, Gaussian Noise, Random Scale, Colouring, Horizontal Flip, Cropping, Rotate. Fig. 3 depicts images after augmentation techniques have been applied.

Our method expands the training and testing sample by including medical slice images with new attributes generated from the fundamental set. By

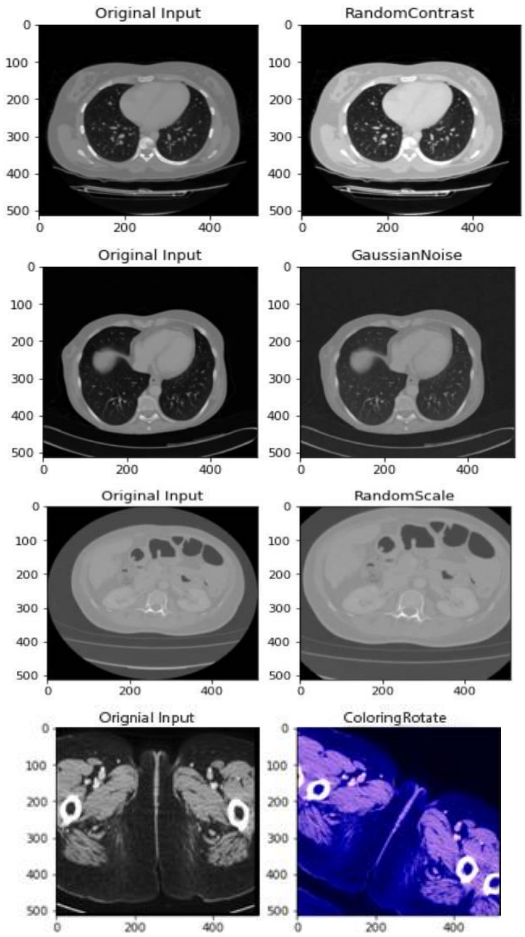

Figure. 3 Examples of the input images from the used datasets after applying augmentation techniques

expanding the data in this manner, it is possible to assess how well the model can distinguish between photos that have been rotated, coloured, cropped, blurred, or enlarged. The models can recognize a form even if it is upside down and can store shapes and provide accurate results when they are in a certain location.

3.3 Proposed learning model

We discovered that all research using deep learning were based on a single model or a comparison of various models in the section on related work. In this research, we combine a number of pre-trained models and exploits the distinct features of each. The essence of computer vision is the traditional machine learning method, which is used to describe and discover features, but it is ineffective for complex classifications and is therefore no longer employed.

When used to classify images, deep learning techniques such as CNNs have made significant contributions to the field of tumour classification. In this study, we compared the performance of two different pre-trained model combinations on the two datasets and then confirmed the best one to be the confirmed model.

Fig. 4 depicts how we combine DeeplapV3 [17] and ResNet-50 [18]. Figure 5 depicts how we combine VGG-16 [19] with ResNet-50V2 [20] and U-Net++ [11].

3.3.1. First proposed model

To take the advantages of pre-trained previous experience and the weights revealed, we utilized DeeplapV3 [17] and ResNet-50 [18] as pre-trained models. The input mage size that fed to our model is 512×512 with total parameters of 17,869,697, which is shown in Figure 6. There are nine blocks in this structure and with ReLU activation function in each block. A 2D convolution and max-pooling layers, and a batch normalisation layer make up the first block. Ten convolution and batch normalisation layers and three additional layers make up the second block. Thirteen convolution layers, four unique layers and thirteen batch normalisation layers make up the third block. The block 4 contains 19 convolution and batch normalisation layers with six adding layers. The following block consists of four layers of convolution, one layer of concatenation, four layers of batch normalisation, and one layer of average pooling. One concatenation layer and two dense layers are followed by a global average 2D pooling layer, and two convolution layers are followed by two batch normalisation layers. The remaining blocks each have a batch normalisation layer with an activation function on top of a layer of 2D convolution. Block 8 also has two dense layers and a global average 2D pooling layer.

The model now includes the following layers:

- Global average 2D pooling layer: The concatenate layer is fully connected for down sampling operation.
- Addition layer: Called the "Add layer", which add the output properties of the layers.
- The neurons from the output rows make up the dense layer type output layer.

3.3.2. Second proposed model

We used VGG-16 [19], ResNet-50V2 [20], and U-Net++ [11] as pre-trained models in this model. Figure 7 depicts the initial portion of the model with input size of 512×512 and the total number of parameters is 4,938,371.

This structure is made up of seven blocks. A 2D convolution layer, a batch normalisation layer, and a 2D average-pooling layer make up each of the first

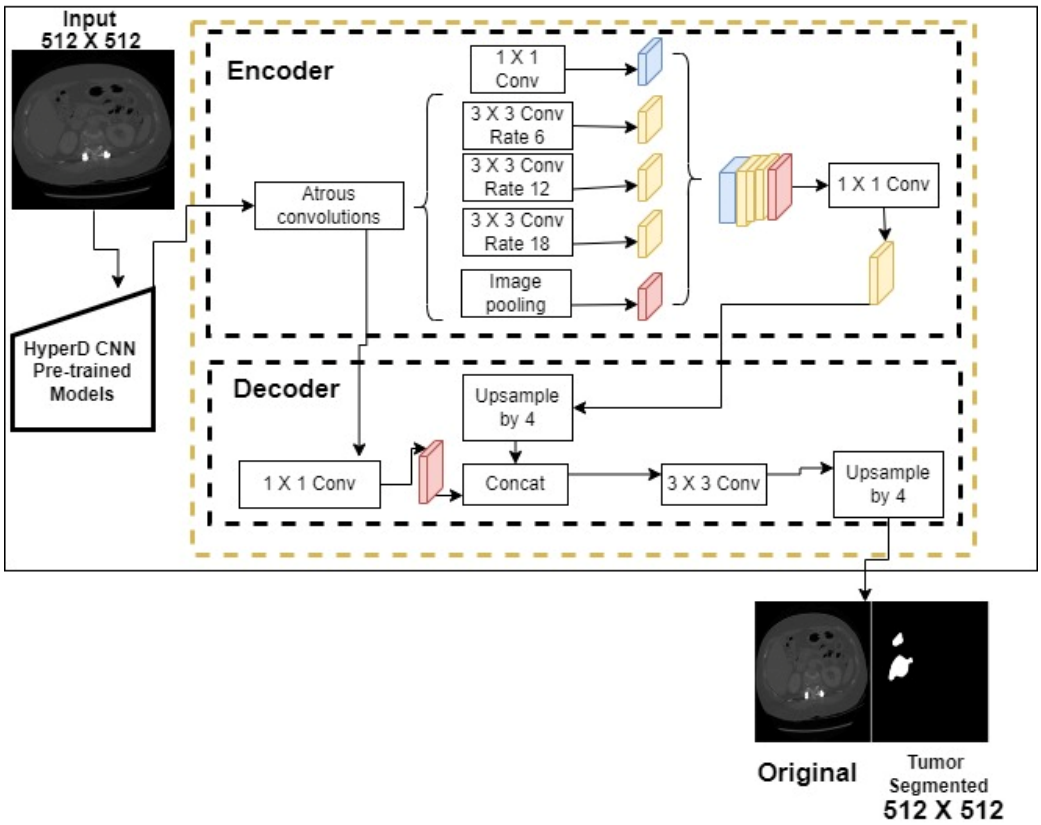

Figure. 4 Block diagram of our first model

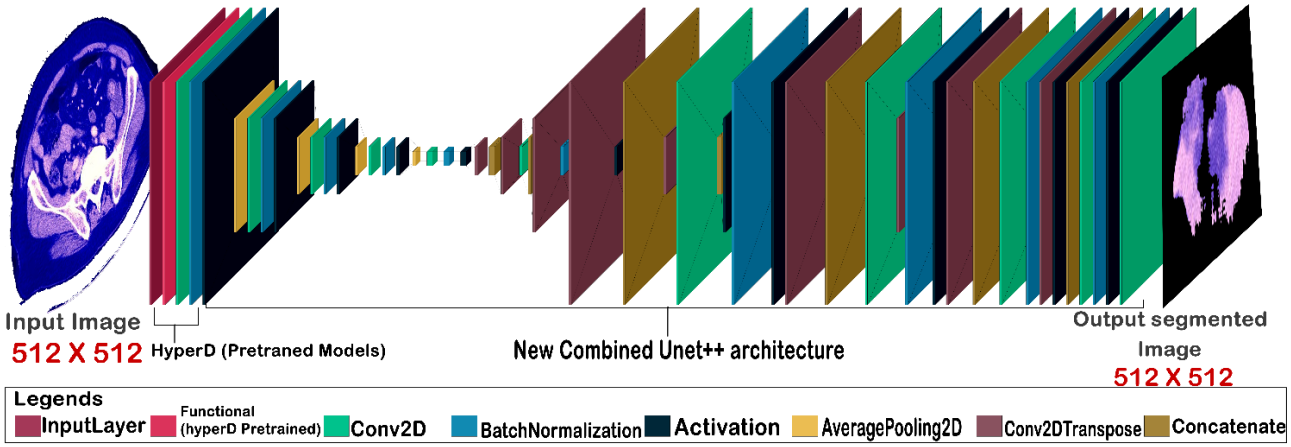

Figure. 5 The structure of the second model

four blocks. A 2D convolution layer, a batch normalisation layer, and a 2D convolution transpose layer with a ReLU activation function make up the fifth building block. This block also includes a concatenation layer and a transposition layer.

A 2D convolution layer, a concatenate layer, and a batch normalisation layer are among the remaining building blocks. The following layers have been supplemented to our model:

- Global average pooling layer: the concatenate layer is fully connected for down sampling operations.
- Transpose layer: This layer inverts the weights by 180 degrees and transposes them; its name is Conv2DTran.
- UNet ++ layers: a newer architecture for segmenting medical images. Decrease semantic gaps between feature maps of encoder and decoder subnetworks by using the re-engineered skip paths.

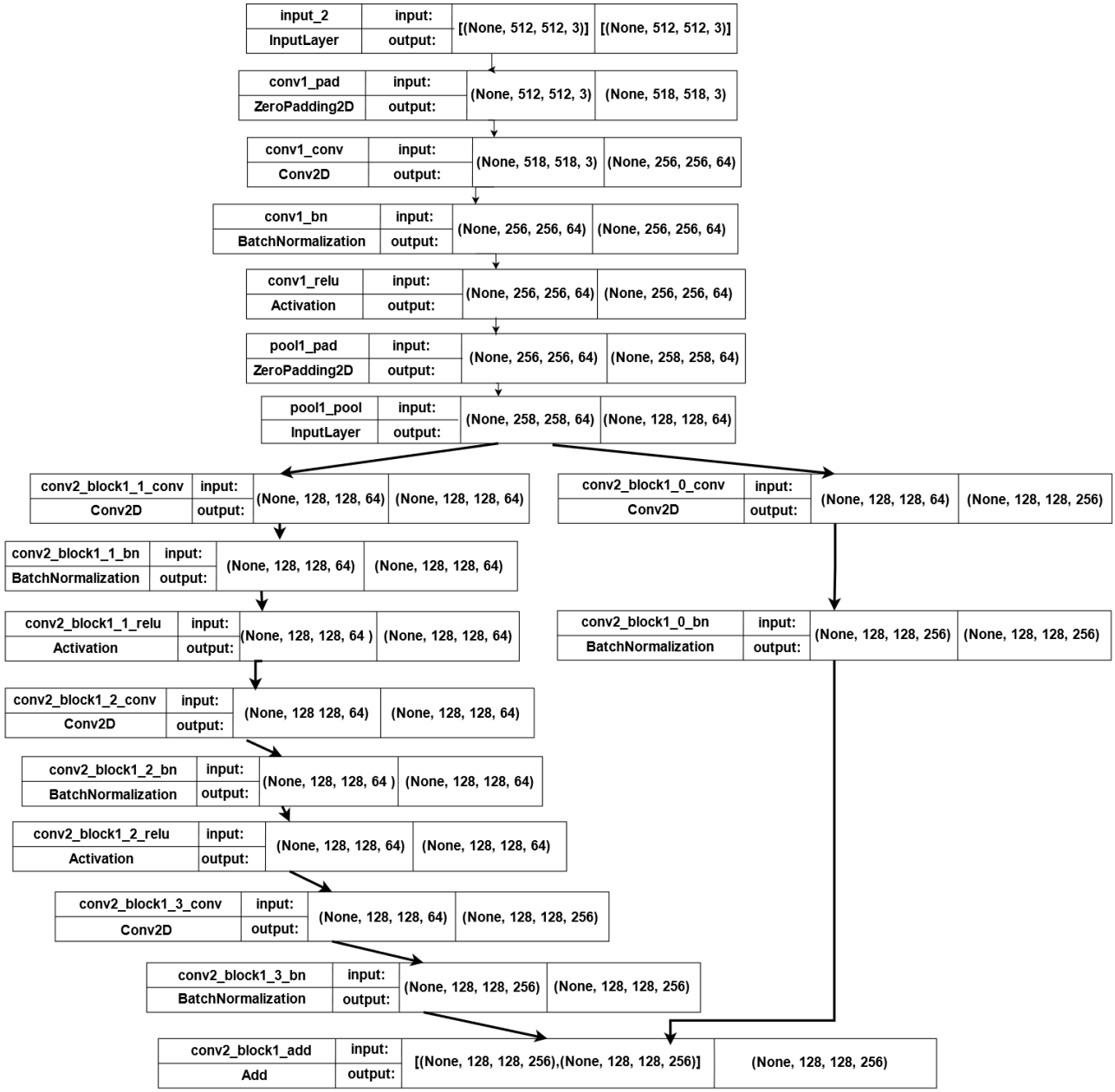

Figure. 6 The first portion of the first model's architecture

4. Experimental results and analysis

The Tensorflow with Keras library was used to run the models in Python. On the two datasets, we tested both models, and the model that performed the best was chosen as our model. Then, we contrasted the confirmed model with other earlier approaches developed in this area.

4.1 Evaluation metrics

To test out our model, we calculate the following evolutions metrics:

i. Calculate the Precision and Recall of our results.
ii. Calculate the Accuracy
iii. Calculate dice coefficient (F1 Score) which are defined as follows:

$$P = \frac{TP}{TP+FP} \quad (1)$$

$$R = \frac{TP}{TP+FN} \quad (2)$$

$$Acc = \frac{TP+TN}{TP+TN+FP+FN} \quad (3)$$

$$dice_{cof} = \frac{2TP}{(2TP+FP+FN)} \quad (4)$$

Figure. 7 The first portion of the second model

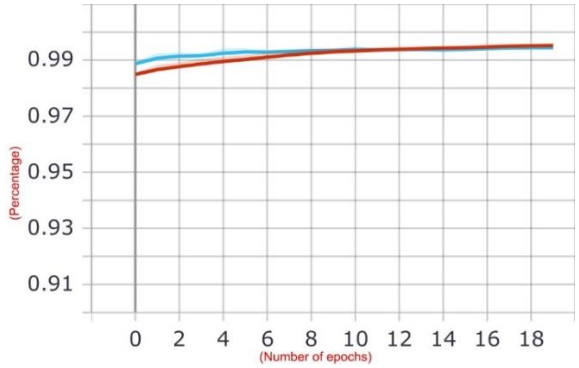

Figure. 8 Over 20 iterations, the validation (blue line) and accuracy (red line) curves of the first model converge

Where P= Precision, R= Recall, Acc= Accuracy, $dice_{cof}$= dice coefficient, TP=True Positives, FP=False Positives, and FN=False Negatives.

4.2 Results on LiTS17 database

4.2.1. The results of our first model

The test set for the dataset was now used to evaluate the first suggested model. Using the previous data and divisions, the model was trained over the course of 20 epochs. The convergence of the accuracy and the validation curve is shown in Fig. 8, which shows that the training has stabilised and accuracy has increased after 8 epochs. By training the model on the training example and comparing the results to the above-mentioned test example, the hidden coefficients for the model's final layer are improved to better matching the images to be trained in each iteration. The model checks images in the validation sample after every training session and achieves a

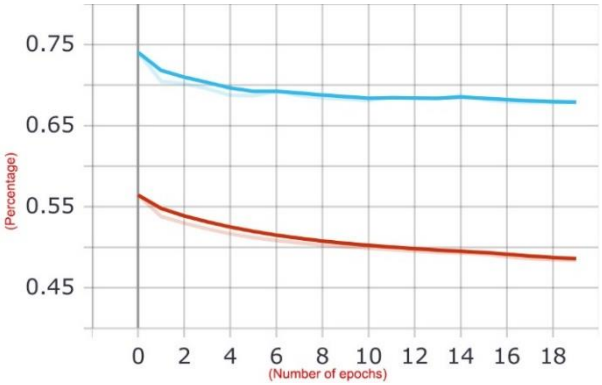

Figure. 9 Validation (blue line) and accuracy (red line) loss curves for the second model during 20 epochs

specific accuracy. This procedure is recurrent for all training epochs, and it was found that in epochs 10 and above, this accuracy does not improve beyond a certain threshold. In our instance, the accuracy was 0.995, meaning that 99.53% of the model's predictions were correct during both the training and validation stages. The loss curve is shown in Fig. 9 as well.

4.2.2. The results of the second proposed model

Using the same test set as the first model, the second proposed model was put to the test. Fig. 11 depicts the model's training process over 20 epochs. After 10 epochs, the training has stabilised and accuracy has increased, according to the drawing of the validation and accuracy curves in the figure.

Visual examples of our results for identifying liver cancer on two images from the dataset are shown in Fig. 10. Consistently, the model checks images in the validation sample after every training session and achieves a specific accuracy. It was found that in phases 18 and above, the accuracy be stable during the end of iteration. The accuracy in our instance was 0.977, meaning that 97.7% of the model's predictions were correct during both the training and validation stages.

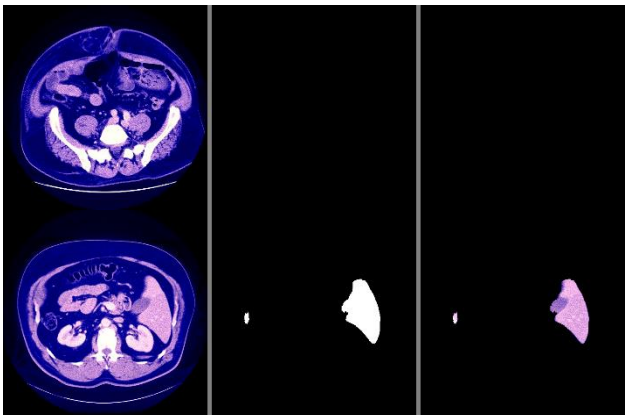

Figure. 10 Visual outcomes of the first cancer detection model (above image is normal case with no tumour detection and other image is abnormal case with tumour detection)

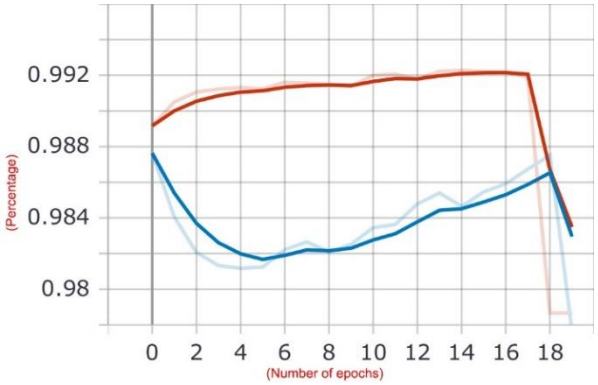

Figure. 11 During 20 iterations, the validation (blue line) and accuracy (red line) curves of the second model

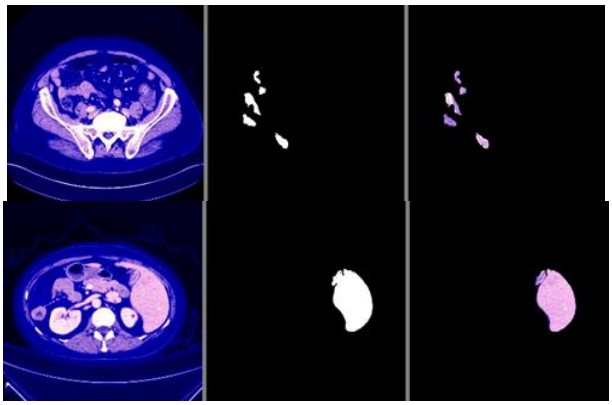

Figure. 12 Visual outcomes of the second cancer detection model (above image is normal case with no tumour detection and other image is abnormal case with tumour detection)

Table 1. In the first dataset, the overall performance of the two models

Model	Acc	P	R	Dice_cof
First	0.995	0.864	0.979	0.516
Second	0.977	0.820	0.580	0.640

Visual samples of our results for identifying liver cancer using our second model on two images are shown in Fig. 12.

Table 1 shows the overall performance of the two models using the metrics from the first dataset.

4.3 Results on 3D-IRCADb-01 dataset

On the second dataset, the same tests are run for the two models (3D-IRCADb-01).

4.3.1. The results of the first model

In this model, the test set—which had been randomly chosen from the second dataset—was used to evaluate the first suggested model. Using the

previous set of data and divisions, the model was trained over 30 iterations. As shown in Fig. 13, the validation and accuracy curve converge, indicating that the training has stabilised and the accuracy has risen after 10 iterations.

As a result of training the model on the training examples, the values of the hidden parameters of the model's final layer have been modified to better match the images to be trained at each stage. It was found that in iteration 15 and above, the accuracy be stable during till the end. In our instance, the accuracy reached 0.995, indicating that 99.5% of the model's accuracy was maintained during the training and validation phases.

4.3.2. The results of our second model

Using the previous set of data and divisions, the model was trained over 60 iterations. As shown in Fig. 14, the validation and accuracy curve converge, indicating that the training has reached a stable state and the accuracy has risen. It was found that in epochs 25 and above, the accuracy be stable during till the end. In our instance, the accuracy reached 0.973, indicating that 97.3% of the model's accuracy was maintained during the training and validation iterations.

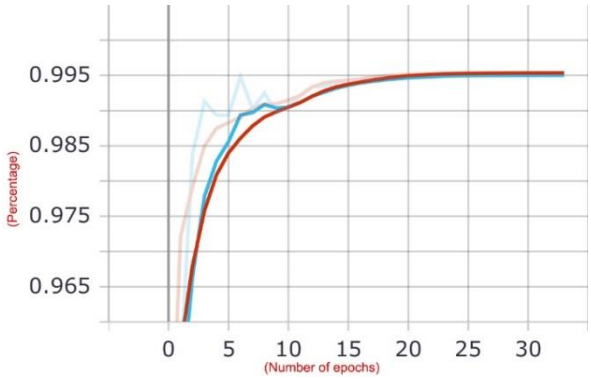

Figure. 13 Over 30 epochs, the validation (blue line) and accuracy (red line) curves of the first model converge

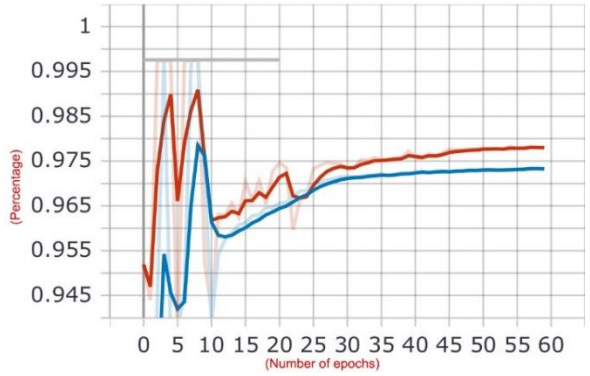

Figure. 14 Over 60 epochs, the validation (blue line) and accuracy (red line) curves of the second model converge

Table 2. In the second dataset, the overall performance of the two models

Model	Acc	P	R	Dice_cof
First	0.995	0.514	0.986	0.561
Second	0.973	0.089	0.977	0.778

Based on the metrics from the second dataset, Table 2 displays the overall performance of the two models.

5. Discussion

Using both datasets, the first proposed method achieved higher accuracies than the second method. This is evident from the previous results. We verified the first approach as our approach as a result. The outcomes also demonstrate that the first method outperformed earlier deep learning techniques in terms of robustness and efficiency, achieving the highest accuracy of 99.5% on small dataset. Additionally, using the first dataset, Figure 10 demonstrates how the first model successfully distinguishes cancer from the healthy image. However, as shown in Fig. 12 (a), the second method exhibits roughly noise when identifying cancer from the normal case. The first model performs better than the second when there is less noise when using the second dataset (small data) to identify cancer from images. In addition, From Table 1, we can show that the first model's ability to predict the positive images from the first dataset is 97.92%. Also, from same Table on the first dataset we can find that, the second model's ability to predict the positive images is 58%. On the second dataset, Table 2 shows that the first model's ability to predict the positive images from the first dataset is 98.60% and the second model is 97.70%. These results also prove the robustness of the first proposed model compared with the second model when working on multi-task classification. Fig. 15 and 16 show the evaluation of recall during the iterations for the first and second model on the first dataset.

From Fig. 15 and 16, we can observe that the first model can predict the true images of the liver cancer better than the second model. From Figure 15, the proposed first model start with 96.5% detecting of the true images during the first 20K iterations and the recall increasing to reach 80K iterations and stable when reaching 140K iteration with an average recall of 98.6%. Whereas the second model is starting with a very low recall during the first 80K iterations with an average recall of 45% and stable when reach to 140K iterations with an average recall of 58%.

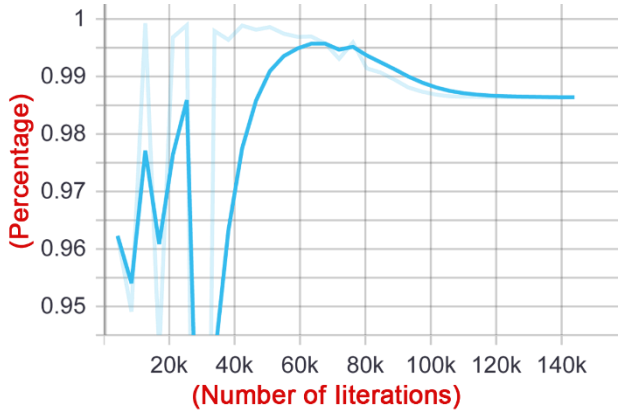

Figure. 15 Evaluation of recall during the iterations for the first model on the first dataset

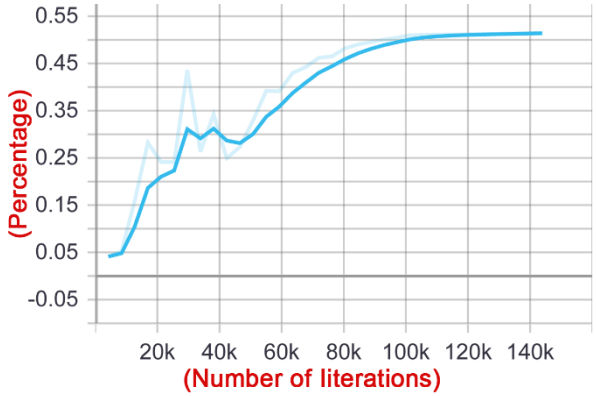

Figure. 16 Evaluation of recall during the iterations for the second model on the first dataset

The reasons of the increasing in the performance of the first model are as follow:

- We employed DeepLabv3, which is used to solve the problem of segmenting objects at various sizes which is better for detecting the liver cancer from the first dataset that contain several images with different scales and also when using augmentation techniques. This is done by applying the Atrous convolution (r) to the input feature map (x) as shown in Eq. (5):

$$y[i] = \sum_k x[i + r.k]w[k] \quad (5)$$

- Other reason of the increasing in the accuracy is the combination with the ResNet, which is desired to solve the degradation issue in a deep network which is better when adding more layers to the network, which causes accuracy to achieve saturation and then decline. Therefore, we can find that the accuracy of the recall of the second model is high when using the second model, which we added more layers than the first one. This residual block F(x) can be represented mathematically as Eq. (6):

$$y = F(x, \{w_i\}) + x \quad (6)$$

where y and x are the output and the input functions to the residual block F(x, {Wi}).

- Finally, in both models, we take the advantages of several pretrained models and try to improve the performance of these pretrained models and try to overcome most of their limitations by adding new layers as mentioned in Section 3. Therefore, the architecture of our models is unique due to the creation of a novel architecture able to exploit the strength of numerous pre-trained models and transfer learning techniques.

The AI-assisted liver cancer detection system helps doctors decide whether a patient is infected or not, significantly reducing the likelihood of incorrect diagnoses and saving the doctor's time and effort by delivering quicker and more accurate results. As a result, it aids in the decline of liver cancer-related fatalities. As a result, various models for detecting liver cancer were presented in several studies [5-10, 21-26]. Several previous approaches were compared with the suggested approach using both datasets as shown in Table 3 and 4.

Havaei *et al*. [5] focused on improving the processing time, not on accuracy, using traditional CNN. Dong *et al*. [6] were able to diagnose cancer with a low accuracy of 97.22%. The method presented by Sureshkumar *et al*. [7] is slower than other neural network models when classifying new cases and require more memory space for the processing. Kaur *et al*. [8] is also Computational complexity and suffer from overfitting problem. The method presented by Shukla et al. [9] is not robust and obtain low performance with big and small data. Also, the method of Ghoniem [10] obtained very low classification results when working on small data. In [21], the authors introduce a method based on modification of the U-Net model for segmentation the liver cancer automatically. In [22], the authors also presented a CNN model that consists of small number of layers and parameters for liver cancer segmentation. Authors in [21, 22], cannot deal with low-contrast boundaries images (as in both datasets) and obtained very low accuracy. As in [21], Kalsoom *et al*. [23] employed a method using modified U-Net but with different structure for liver tumour detection. They obtained a very low accuracy when working on big data. A novel and efficient integration method for the detection of liver tumours is presented in this paper to overcome the issues of the previous works. The proposed method outperforms the majority of existing algorithms on both small and large datasets. Additionally,

compared to earlier low-resource deep learning methods for liver detection, our approach is more robust.

Despite the fact that there have been many contributions in this area, each one has concentrated on using a single neural network to identify cancer. No attempt has been made to combine several models in order to benefit from the unique qualities of each model. Additionally, whereas our method produced excellent results with small data, the majority of earlier works produced poor results with small data.

In numerous ways, our methods have several limitations. CT scans were shrunk to appropriate the Nvidia 1080 Ti GPU (8 GB Memory). Future research will be able to train models with big data or maintain the original image resolution without downscaling. By retaining the full resolution of CT scan images, the segmented tumour region will be displayed in greater detail, and performance is likely to be enhanced. The used datasets in this paper did not contain all cancer tumours, and radiologists' evaluations were used to label the images contained within the datasets. Future research on radiologists-missed interval liver cancers and MRI datasets would be useful for training algorithms to detect non-visible cancerous tumours. The LITS and 3D-IRCADb-01 datasets lacked samples that were nationally representative. Therefore, these performance measures cannot be directly compared to national estimates of the sensitivity and specificity of radiologists. A large number of weight parameter constraints led to a large model size and extended inference time in the research.

6. Conclusion

The main goal of this paper is to propose novel two combination systems using several deep learning models for the detection of liver cancer. The architecture of our models is unique due to the creation of a novel architecture able to exploit the strength of numerous pre-trained models and transfer learning techniques. In order to learn using several pre-trained models and integrate the results of each of these networks' final layers, we selected the model that performed the best. In order to recognise images of liver tumours, modify this model next. The proposed model's accuracy on both datasets was 99.5%, which is better than the outcomes of other methods applied to this area. The suggested method can be applied to the system for diagnosing and treating liver cancer, assisting clinicians in better surgical planning for patients with liver cancer. We intend to develop our model in the future to enhance performance and deliver a more precise classification. In order to evaluate the model's accuracy, we also plan to test it on various cancer types.

Table 3. Performance comparison between the selected model and other earlier models using LiTS17 database (our results in **bold**)

Reference/ Year	Approach	Performance (%)
[21] 2022	RIU-Net	Dice_cof = 73.79
[22] 2022	CNN	Acc = 97.25
[10] 2020	artificial bee colony optimization + UNet Network	Acc = 98.50
[8] 2021	CNN	Acc = 99.10
Proposed 2022	**Hyperion Pre-trained Models**	**Acc = 99.50**

Table 4. Performance comparison between the selected model and other earlier models using 3D-IRCADb-01 database (our results in **bold**)

Reference/ Year	Approach	Performance (%)
[21] 2022	RIU-Net	Dice_cof = 76.55
[22] 2022	CNN	Acc = 93.10
[23] 2022	modified U-Net	Acc = 93
[24] 2022	HPM-Net	Acc = 98.88
[25] 2021	Dense V-Net	Dice_cof = 76.93
[26] 2022	FC-CNN	Acc = 99.11
[9] 2022	CNN	Acc = 94.21
Proposed 2022	**Hyperion Pre-trained Models**	**Acc = 99.50**

Conflicts of Interest

The authors declare no conflict of interest.

Author Contributions

Conceptualization, Muhammad Mahmoud and Mina Ibrahim; methodology, Muhammad Mahmoud and Mina Ibrahim; software, Muhammad Mahmoud; validation, Hatem Abdulkader and Reda M. Albadawy; formal analysis, Hatem Abdulkader and Mina Ibrahim; data curation, Muhammad Mahmoud and Reda M. Albadawy; writing—original draft preparation, Muhammad Mahmoud and Mina Ibrahim; writing—review and editing, All; supervision, Hatem Abdulkader, Reda M. Albadawy and Mina Ibrahim.

References

[1] M. H. C. Ramírez, M. R. M. Jiménez, R. F. G. Laredo, J. A. G. Infante, and N. E. R. Guzmán, "Lupane-type triterpenes and their anti-cancer activities against most common malignant tumors: A review", *EXCLI Journal*, Vol. 15, p. 758, 2016.

[2] K. Kinkel, Y. Lu, M. Both, R. S. Warren, and R. F. Thoeni, "Detection of hepatic metastases from cancers of the gastrointestinal tract by using noninvasive imaging methods (US, CT, MR imaging, PET): a meta-analysis", *Radiology*, Vol. 224, No. 3, pp. 748-756, 2002.

[3] Y. S. Mohammed, H. Abdelkader, P. Pławiak, and M Hammad, "A novel model to optimize multiple imputation algorithm for missing data using evolution methods", *Biomedical Signal Processing and Control*, Vol. 76, p. 103661, 2022.

[4] W. Książek, M. Hammad, P. Pławiak, U. R. Acharya, and R. Tadeusiewicz, "Development of novel ensemble model using stacking learning and evolutionary computation techniques for automated hepatocellular carcinoma detection", *Biocybernetics and Biomedical Engineering*, Vol. 40, No. 4, pp. 1512-1524, 2020.

[5] M. Havaei, A. Davy, D. W. Farley, A. Biard, A. Courville, Y. Bengio, C. Pal, P. M. Jodoin, and H. Larochelle, "Brain tumor segmentation with deep neural networks", *Medical Image Analysis*, Vol. 35, pp. 18-31, 2017.

[6] X. Dong, Y. Zhou, L. Wang, J. Peng, Y. Lou, and Y. Fan, "Liver cancer detection using hybridized fully convolutional neural network based on deep learning framework", *IEEE Access*, Vol. 8, pp. 129889-129898, 2020.

[7] V. Sureshkumar, V. Chandrasekar, R. Venkatesan, and R. K. Prasad, "Improved performance accuracy in detecting tumor in liver using deep learning techniques", *Journal of Ambient Intelligence and Humanized Computing*, Vol. 12, No. 6, pp. 5763-5770, 2021.

[8] A. Kaur, A. P. Singh, and A. K. Aggarwal, "An automated slice sorting technique for multi-slice computed tomography liver cancer images using convolutional network", *Expert Systems with Applications*, Vol. 186, p. 115686, 2021.

[9] P. K. Shukla, M. Zakariah, W. A. Hatamleh, H. Tarazi, and B. Tiwari, "AI-DRIVEN novel approach for liver cancer screening and prediction using cascaded fully convolutional neural network", *Journal of Healthcare Engineering*, Vol. 2022, 2022.

[10] R. M. Ghoniem, "A novel bio-inspired deep learning approach for liver cancer diagnosis", *Information*, Vol. 11, No. 2, p. 80, 2020.

[11] Z. Zhou, M. M. R. Siddiquee, N. Tajbakhsh, and J. Liang, "Unet++: A nested u-net architecture for medical image segmentation", *In Deep Learning in Medical Image Analysis and Multimodal Learning for Clinical Decision Support*, pp. 3-11, 2018.

[12] O. Ronneberger, P. Fischer, and T. Brox, "U-net: Convolutional networks for biomedical image segmentation", In: *Proc. of International Conference on Medical Image Computing and Computer-Assisted Intervention*, pp. 234-241. 2015.

[13] M. Rela, N. R. Suryakari, and P. R. Reddy, "Liver tumor segmentation and classification: A systematic review", *IEEE HYDCON*, Vol. 2020, pp. 1-6, 2020.

[14] A. A. Aatresh, K. Alabhya, S. Lal, J. Kini, and P. U. Saxena, "LiverNet: efficient and robust deep learning model for automatic diagnosis of sub-types of liver hepatocellular carcinoma cancer from H&E stained liver histopathology images", *International Journal of Computer Assisted Radiology and Surgery*, Vol. 16, No. 9, pp. 1549-1563, 2021.

[15] P. Bilic, P. F. Christ, E. Vorontsov, G. Chlebus, H. Chen, Q. Dou, C. W. Fu, X. Han, P. A. Heng, J. Hesser, and S. Kadoury, "The liver tumor segmentation benchmark (lits)", *arXiv Preprint arXiv:1901.04056*, 2019.

[16] L. Soler, A. Hostettler, V. Agnus, A. Charnoz, J. Fasquel, J. Moreau, A. Osswald, M. Bouhadjar, and J. Marescaux, "3D image reconstruction for comparison of algorithm database: A patient specific anatomical and medical image

database", *IRCAD, Strasbourg, France, Tech. Rep.*, Vol. 1, No. 1, 2010.

[17] S. C. Yurtkulu, Y. H. Şahin, and G. Unal, "Semantic segmentation with extended DeepLabv3 architecture", In: *Proc. of 2019 27th Signal Processing and Communications Applications Conference (SIU)*, pp. 1-4. 2019.

[18] Q. A. A. Haija and A. Adebanjo, "Breast cancer diagnosis in histopathological images using ResNet-50 convolutional neural network", In: *Proc. of 2020 IEEE International IOT, Electronics and Mechatronics Conference (IEMTRONICS)*, pp. 1-7. 2020.

[19] S. Tammina, "Transfer learning using vgg-16 with deep convolutional neural network for classifying images", *International Journal of Scientific and Research Publications (IJSRP)*, Vol. 9, No. 10, pp. 143-150, 2019.

[20] P. Sertic, A. Alahmar, T. Akilan, M. Javorac, and Y. Gupta, "Intelligent Real-Time Face-Mask Detection System with Hardware Acceleration for COVID-19 Mitigation", *Healthcare*, Vol. 10, No. 5, p. 873. 2022.

[21] P. Lv, J. Wang, and H. Wang, "2.5 D lightweight RIU-Net for automatic liver and tumor segmentation from CT", *Biomedical Signal Processing and Control*, Vol. 75, p. 103567, 2022.

[22] M. Ahmad, S. F. Qadri, S. Qadri, I. A. Saeed, S. S. Zareen, Z. Iqbal, A. Alabrah, H. M. Alaghbari, M. Rahman, and S. Md, "A lightweight convolutional neural network model for liver segmentation in medical diagnosis", *Computational Intelligence and Neuroscience*, Vol. 2022, 2022.

[23] A. Kalsoom, M. Maqsood, S. Yasmin, M. Bukhari, Z. Shin, and S. Rho, "A computer-aided diagnostic system for liver tumor detection using modified U-Net architecture", *The Journal of Supercomputing*, Vol. 78, No. 7, pp. 9668-9690, 2022.

[24] W. Hao, J. Zhang, J. Su, Y. Song, Z. Liu, Y. Liu, C. Qiu, and K. Han, "HPM-Net: Hierarchical progressive multiscale network for liver vessel segmentation in CT images", *Computer Methods and Programs in Biomedicine*, Vol. 224, p. 107003, 2022.

[25] J. Su, Z. Liu, J. Zhang, V. S. Sheng, Y. Song, Y. Zhu, and Y. Liu, "DV-Net: Accurate liver vessel segmentation via dense connection model with D-BCE loss function", *Knowledge-Based Systems*, Vol. 232 p. 107471, 2021.

[26] S. H. Vadlamudi, Y. S. S. Reddy, P. A. S. K. Reddy, P. Periasamy, and N. M. V. Mohamad, "Automatic liver tumor segmentation and identification using fully connected convolutional neural network from CT images", *Concurrency and Computation: Practice and Experience*, p. e7212, 2022.